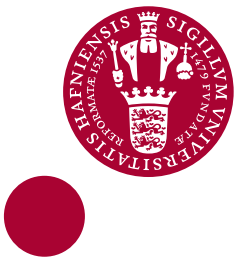

Characterization of Polymer Blends

Miscibility, Morphology and Interfaces

Mortensen, Kell

Published in:
Characterization of Polymer Blends and Block Copolymers by Neutron Scattering

Publication date:
2014

Document version
Early version, also known as pre-print

7
Characterization of Polymer Blends and Block Copolymers by Neutron Scattering: Miscibility and Nanoscale Morphology

Kell Mortensen

7.1
Introduction

The interaction between materials and radiation takes a variety of forms, including absorption and fluorescence, refraction, scattering and reflection. These types of interaction are all tightly related in terms of physical quantities. In this chapter, attention will be focused on the scattering term, when used to determine materials' properties such as miscibility and nanoscale structure. The method relies on the wave-character of the radiation; this is the case whether using electromagnetic beams of light or X-rays with oscillating electric and magnetic fields, or particle radiation such as neutrons or electrons. In the latter cases, it is the de Broglie wave character of the particles that is the relevant quantity.

Insight into structural properties using scattering techniques appears as a result of the interference between radiation that is scattered from different sites in the sample. A simple illustration is given in the Young interference experiment, shown in Figure 7.1, where the radiation of plane waves propagate through two slits, making an interference pattern that depend on the separation distance between the two slits, and the wavelength of the radiation.

7.2
Small-Angle Scattering

The principle of small-angle scattering is illustrated schematically in Figures 7.2 and 7.4. A sample is placed in a collimated, monochromatic beam and the scattered beam is monitored. The detected scattering pattern reflects the structural properties of the sample. Small-angle scattering by X-rays (SAXS) or by neutrons (SANS) are ideal techniques for studying structures on the length scale of 1 to 500 nm, that is, nanoscale structural properties such as macromolecules, nanoparticles or molecular density fluctuations. Neutron sources for SANS experiments may be either continuous (typical for reactor sources) or pulsed (typical for spallation sources). For the pulsed sources, the demand for a monochromatic beam

Characterization of Polymer Blends: Miscibility, Morphology, and Interfaces, First Edition.
Edited by S. Thomas, Y. Grohens, and P. Jyotishkumar.

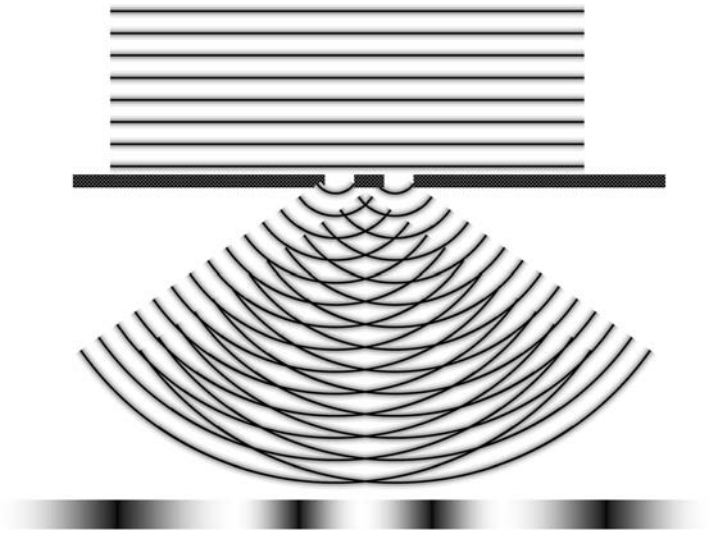

Figure 7.1 Experiments using scattering methods rely on interference between wave-like radiation, here illustrated schematically in Young's two-slit experiment.

can be obtained using the time-profile of the elastic scattered beam, or the beam can be monochromatized as required in the reactor case. SAXS instruments may be either laboratory instruments based on an irradiated anode source, or located at synchrotron facilities.

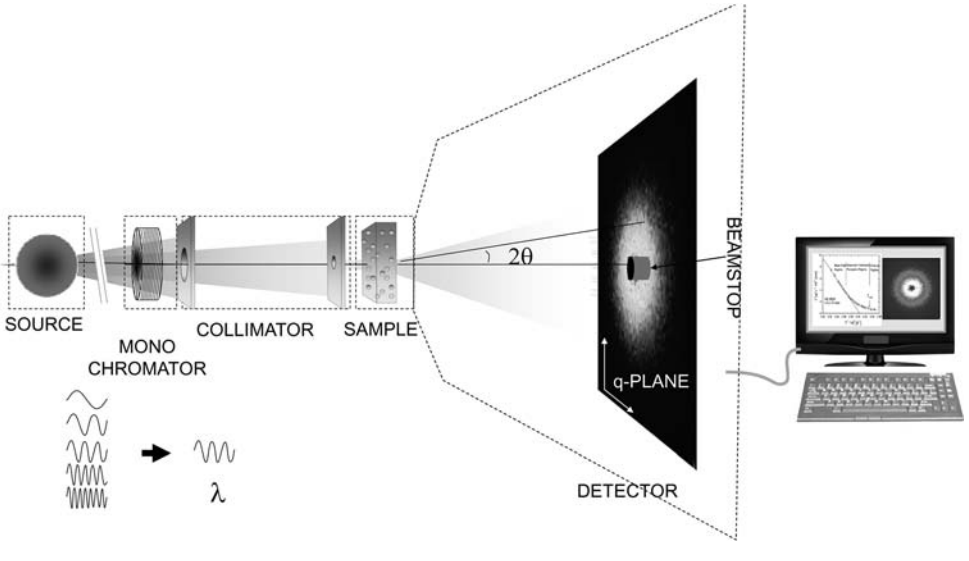

Figure 7.2 Illustration of small-angle scattering.

The scattered beam is, beyond trivial factors such as incoming flux, transmission and geometric factors, proportional to two terms: (i) a contrast factor reflecting the ability of individual atoms to interact with the radiation; and (ii) the structure factor resulting from interference effects of scattering originating from different sites in the sample, providing information on structural properties.

Reflectometry is somewhat related to small-angle scattering, especially grazing-incidence reflectometry. Simple reflectometry measures the reflected beam from a surface or interface of the sample investigated.

7.2.1 Contrast

In order to measure structural properties, there must be difference between the ability to scatter radiation from the characteristic elements to be studied. There must also be a contrast, as seen by the applied radiation.

Neutrons are probably best known as elementary particles that comprise the nuclei of atoms. Typical nuclei contain approximately similar numbers of protons and neutrons. The free neutron has, as any particle, an associated wavelength determined by the mass, m_n, and the velocity, v_n, according to the de Broglie relation:

$$\lambda_n = \frac{h}{m_n v_n}$$

where h is Planck's constant. At ambient temperatures, $T = 300\,\mathrm{K}$, $v_n = \sqrt{k_B T/m_n} \approx 3000\,\mathrm{m\,s^{-1}}$ giving the thermal neutron wavelength: $\lambda_n = 1.4\,\text{Å}$. This value, which is of the same order of magnitude as that of X-radiation, makes neutrons effective as structural probes on the nanometer length scale.

The interaction between neutrons and matter is complex, and includes magnetic terms as the neutron itself is magnetic. The interaction between a neutron and a nuclei can generally not be calculated *ab initio*, but is given in tables based on experimental values of scattering lengths and scattering cross-sections. The interaction between the electrons and the neutron is primarily via the magnetic moment. The magnetic interaction makes neutron scattering ideal for studying magnetic structures and fluctuations.

For nonmagnetic materials, the magnetic moments of the nuclei are completely uncorrelated. The magnetic scattering is therefore not coherent, but gives rise to an isotropic incoherent background that may be quite large for some materials. An important example here is hydrogen $^{1}\mathrm{H}$, which has a large incoherent scattering contribution. Oxygen $^{16}\mathrm{O}$ and carbon $^{12}\mathrm{C}$, on the other hand, are examples of elements that produce very little incoherent background due to the vanishing magnetic moment in these nuclei.

The nonmagnetic interaction gives rise to coherent scattering, where interference effects are effective. This is the part of the scattering that provides insight into the structural properties. The interaction with neutrons not only depends on the atomic number within the periodic system; indeed, different

Table 7.1 Scattering length and incoherent scattering cross-section of typical nuclei of soft matter materials. Nuclei with no index represent natural, mixed isotopes [http://www.ncnr.nist.gov/resources/n-lengths].

Nuclei	Coherent scattering length	Incoherent cross-section
	b	σ_{ic}
H	-0.3739×10^{-12} cm	80.26×10^{-24} cm^2
^{1}H	-0.3741×10^{-12} cm	80.27×10^{-24} cm^2
^{2}H = D	0.6671×10^{-12} cm	2.05×10^{-24} cm^2
C	0.6646×10^{-12} cm	0.001×10^{-24} cm^2
N	0.936×10^{-12} cm	0.5×10^{-24} cm^2
O	0.5803×10^{-12} cm	0.0×10^{-24} cm^2
Si	0.4149×10^{-12} cm	0.004×10^{-24} cm^2

isotopes of the same atom may have significantly different abilities to scatter neutrons, and even different signs in the related scattering length, b. A most important example of this is hydrogen, where the most common ^{1}H isotope (H) and the heavy hydrogen counterpart, ^{2}H, deuterium (D) have significant different scattering lengths: $b_H = -0.3739 \times 10^{-12}$ cm and $b_D = 0.6671 \times 10^{-12}$ cm. The scattering lengths and incoherent scattering cross-sections for selected isotopes are listed in Table 7.1.

Chemically, the two hydrogen isotopes are similar, and specific structural identities can thereby be highlighted by replacing H with D at given chemical sites; specific units can be "colored" to make them visible in the neutron beam.

Important examples using deuterium labeling include polymer melts, where individual polymer coils can be highlighted by mixing similar polymers with respectively H and D atoms in the chain; this is illustrated in Figure 7.3.

The characteristics of small-angle scattering does not allow atomic resolution. It is desirable, therefore, to substitute the nuclear scattering lengths, b, with a continuous *scattering length density* function, ρ, which averages the b-values over an appropriate volume V, which should be small compared to the instrumental resolution. ρ is thus defined as

$$\rho = \frac{1}{V}\sum_V b_i = \frac{N_A \delta}{M_V}\sum_V b_i \tag{7.1}$$

which is summed over the nuclear b_i-values within the volume V. N_A is Avogadro's number, δ the mass density, and M_V the molar mass corresponding to the chosen volume. For a liquid, one would typically calculate ρ based on the sum over a single solvent molecule, while for a polymer it would be that of the monomer unit.

For X-rays, the interaction between radiation and matter is primarily via interaction between the electrons and the oscillatory electric field of the electromagnetic beam. $E = E_\circ \cos(\omega t)$. An electron will, in the X-ray beam, be accelerated by the oscillating electric field; an accelerated charged particle, on the other hand, will

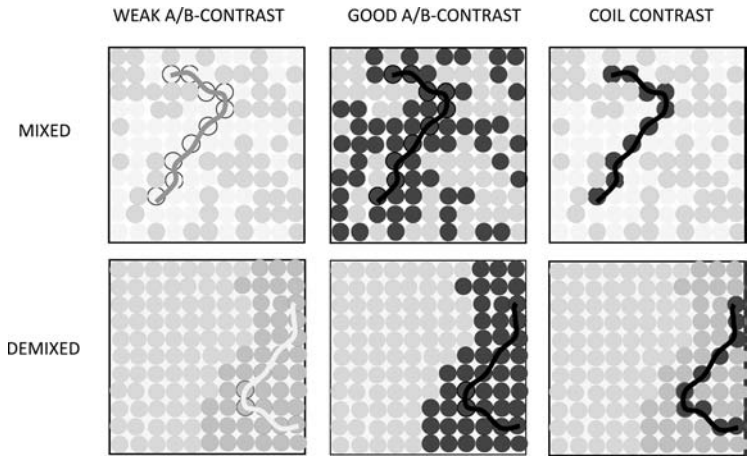

Figure 7.3 Neutron scattering contrasts of polymer blend, illustrating good and weak contrast. The weak contrast examples illustrate the contrast within typical polymer blends. The good contrast example illustrates how contrast between the A and B-polymers can be enhanced using D-labeling. The coil contrast example shows how "single" coils can be labeled to study the conformation of individual polymer chains in the mixed and in the demixed states. The units may be interpreted as the Kuhn-length of the polymer chain.

irradiate radiation itself with frequency equal to the accelerating field. The result is X-ray irradiated from the electron:

$$\mathbf{E}_{\text{rad}} \propto -\frac{e^2}{m_e c^2}\frac{\mathbf{E}}{r} \tag{7.2}$$

The pre-factor in Eq. (7.2) is the scattering length, b, for an individual electron, that is,

$$b_e = -\frac{e^2}{m_e c^2} = 0.282 \times 10^{-4}\,\text{A} \tag{7.3}$$

with the dimension of length. b_e of the electron is also called the Thompson scattering length. To obtain the scattering of an atom, it is necessary to integrate over all electrons in the atom which, for small angles (small $\mathbf{q}$) approach b_e times the number of electrons, that is,

$$b_{\text{atom}} \approx b_e \cdot Z.$$

Different polymers have typically rather similar electron densities, giving only weak X-ray contrasts. Neutron scattering is therefore usually superior for studying the thermodynamics of polymer blends, using specific deuterium labeling.

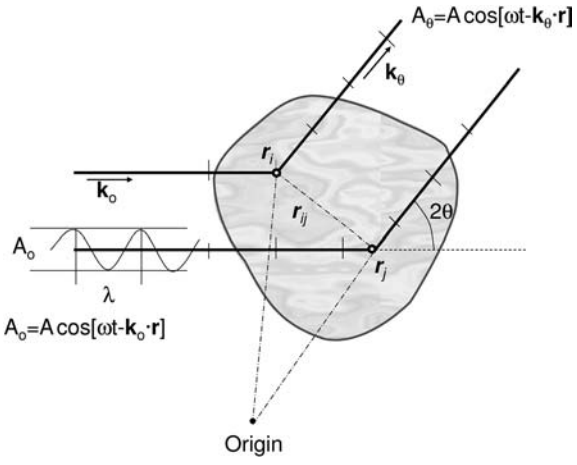

Figure 7.4 Phase difference for scattering from different sites into given angle 2θ.

7.2.2 Scattering Function

Figure 7.4 describes schematically the radiation scattered into a given angle 2θ from two sites in the sample, $\mathbf{R}_i$ and $\mathbf{R}_j$. The incoming radiation is characterized by the wavelength λ and direction given by wave vector $\mathbf{k}_\circ$.

The elastically scattered wave has the same wavelength, and we consider the term scattered into a given angle 2θ defined by the scattered wave vector $\mathbf{k}_\theta$. The phase difference $\Delta\phi$ between radiation origination from the two sites $\mathbf{R}_i$ and $\mathbf{R}_j$ is, from the figure, seen to be $2\pi/\lambda$ times the path length difference, which may be expressed as

$$\Delta\phi = \mathbf{r}_{ij} \cdot (\mathbf{k}_\theta - \mathbf{k}_\circ) = \mathbf{r}_{ij} \cdot \mathbf{q} \tag{7.4}$$

where $\mathbf{r}_{ij} = \mathbf{R}_i - \mathbf{R}_j$, and $\mathbf{q} \equiv (\mathbf{k}_\theta - \mathbf{k}_\circ)$ is the *scattering vector*. The numerical value of $\mathbf{q}$ is

$$q = |\mathbf{q}| = \frac{4\pi}{\lambda}\sin\theta \tag{7.5}$$

The radiation is for light, X-ray and neutrons expressed in terms of a plane wave with amplitude oscillating in time (t) and space ($\mathbf{R}$) which, using complex notation, is expressed as

$$A(\mathbf{R}, t) = A_\circ \exp[i(\omega t - \mathbf{k} \cdot \mathbf{R})] \tag{7.6}$$

where the real part of Eq. (7.6) reflects the physical value. The radiation scattered from various sites may vary, thus reflecting the ability for different atoms to interact with the beam. The probability that the plane wave is scattered from a given site $\mathbf{R}_i$ of the sample is defined in terms of the scattering length density, ρ, as discussed above.

The amplitude of the radiation at a site $\mathbf{R}$ and time t scattered from a point $\mathbf{R}_i$ into the angle 2θ (i.e., with wave vector $\mathbf{k}_\theta$ and momentum transfer $\mathbf{q}$) depends on the ability to scatter at the site $\mathbf{R}_i$ ($\rho(\mathbf{R}_i)$) and the phase is given by the specific scattering site $\Delta\phi_i = \mathbf{R}_i \cdot \mathbf{q}$:

$$\begin{aligned} A(\mathbf{q})_{\mathbf{R}_i} &= A_\circ \rho(\mathbf{R}_i) \exp[i(\omega t - \Delta\phi_i - \mathbf{k}_\theta \cdot \mathbf{R})] \\ &= A_\circ \rho(\mathbf{R}_i) \exp[-i(\mathbf{q} \cdot \mathbf{R}_i)] \exp[i(\omega t - \mathbf{k}_\theta \cdot \mathbf{R})] \end{aligned} \tag{7.7}$$

The phase-factor $\exp[i\,\mathbf{q} \cdot \mathbf{R}_i]$ explicitly gives the phase relative to that of the non-interacting beam. The total radiation amplitude scattered into a given scattering vector $\mathbf{k}_\theta$, that is, a scattering momentum $\mathbf{q}$, is the simple sum over all sites in the sample:

$$A(\mathbf{q}) = \sum_{\mathbf{R}_i} A(\mathbf{q})_{\mathbf{R}_i} = A_\circ \sum_{sample} \rho(\mathbf{R}_i) \exp[-i(\mathbf{q} \cdot \mathbf{R}_i)] \exp[i(\omega t - \mathbf{k}_\theta \cdot \mathbf{R})] \tag{7.8}$$

Now, it is only possibly to measure beam-intensity, but not the direct in time and space oscillating wave. The intensity is equal to the numerically squared value of $|A(\mathbf{q})|$ or, in complex numbers, the product of $A(\mathbf{q})$ and the complex conjugated $A(\mathbf{q})^*$. Moreover, we measure the ensemble average, thus giving:

$$\tilde{I}(\mathbf{q}) = I_\circ \sum_i \sum_j \langle \rho(\mathbf{R}_i) \rho(\mathbf{R}_j) \exp[-i(\mathbf{q} \cdot \mathbf{r}_{ij})] \rangle \tag{7.9}$$

with $A_\circ^2 = I_\circ$ equal to the intensity of the incoming beam, and where $\langle \ldots \rangle$ denotes ensemble average. Now, let us normalize with respect to $I_\circ$, giving the scattering function:

$$I(\mathbf{q}) = \sum_i \sum_j \langle \rho(\mathbf{R}_i) \rho(\mathbf{R}_j) \exp[-i(\mathbf{q} \cdot \mathbf{r}_{ij})] \rangle \tag{7.10}$$

Let us further substitute the summations with integrals using that $\rho(\mathbf{R})$ can be treated as a continuous function. The scattering function Eq. (7.10) can then be reformulated into integral-form, expressed as

$$\begin{aligned} I(\mathbf{q}) &= \int_{\mathbf{R}_i} \int_{\mathbf{R}j} \langle \rho(\mathbf{R}_i) \rho(\mathbf{R}_j) \rangle \exp[-i\mathbf{q} \cdot \mathbf{r}_{ij}] d\mathbf{R}_j \, d\mathbf{R}_i \\ &= \int_{\mathbf{R}} \int_{\mathbf{r}} \langle \rho(\mathbf{R}) \rho(\mathbf{R} + \mathbf{r}) \rangle \exp[-i\mathbf{q} \cdot \mathbf{r}] d\mathbf{r} \, d\mathbf{R} \end{aligned} \tag{7.11}$$

where $\mathbf{R}_i$ and $\mathbf{R}_j$ are substituted with respectively $\mathbf{R}$ and $\mathbf{R} + \mathbf{r}$. The averaged correlation function $\langle \rho(\mathbf{R}) \rho(\mathbf{R} + \mathbf{r}) \rangle$ does not depend on the specific sites $\mathbf{R}$ and $\mathbf{R} + \mathbf{r}$, but only on the distance $\mathbf{r}$. The $\mathbf{R}$-integral of Eq. (7.11) can thus be eliminated, thereby giving

$$\begin{aligned} I(\mathbf{q}) &= V \cdot \int \langle \rho(\mathbf{R}) \rho(\mathbf{R} + \mathbf{r}) \rangle \exp[-i\mathbf{q} \cdot \mathbf{r}] d\mathbf{r} \\ &= V \cdot \int \gamma(\mathbf{r}) \exp[-i\mathbf{q} \cdot \mathbf{r}] d\mathbf{r} \end{aligned} \tag{7.12}$$

with the correlation function $\gamma(\mathbf{r}) \equiv \langle \rho(\mathbf{R}) \rho(\mathbf{R} + \mathbf{r}) \rangle$. We thus see that, mathematically, the scattering function is the Fourier transform of the ensemble-averaged correlation function $\gamma(\mathbf{r})$ correlating densities separated by distances $\mathbf{r}$. For an isolated polymer chain, the correlation function describes the probability of finding segments of the chain separated by a distance $\mathbf{r}$. In experimental systems this

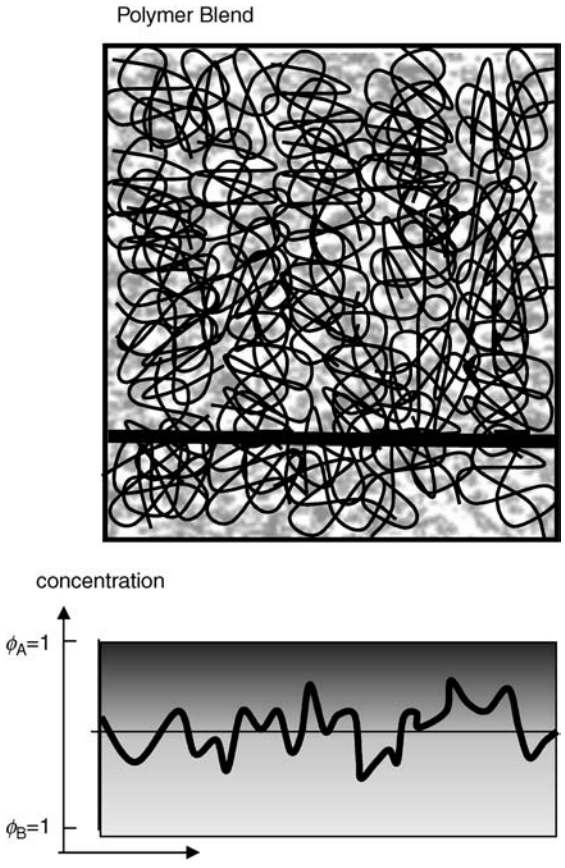

Figure 7.5 Composition fluctuations in a polymer blend illustrated by blends of black and grey chains.

may be polymer chains in dilute solution, or few labeled chains in an environment of nonlabeled (see Figure 7.3). In polymer blends, the correlation function describes the spatial correlation of concentration fluctuations, as illustrated in Figure 7.5.

7.2.3 Gaussian Chain

The conformation of ideal polymer chains corresponds to that of a *random walk*. The mutual distance between segments within the chain obey Gaussian statistics [1]. The size of polymer chains is often given in terms of the *end-to-end distance*, $R_\circ$, or the *radius of gyration*, R_g. The radius of gyration is experimentally accessible from scattering experiments.

The end-to-end vector is given by

$$\mathbf{R}_\circ = \sum_{i=1}^{N} \mathbf{R}_i \tag{7.13}$$

where N is the number of Kuhn-segments (proportional to the degree of polymerization) and $\mathbf{R}_i$ is the vector of the i-th segment. For an isotropic collection of chains the average end-to-end vector must be zero: $\langle \mathbf{R}_\circ \rangle = 0$. The mean-square end-to-end distance, on the other hand, is non-zero:

$$\langle \mathbf{R}_\circ^2 \rangle = \sum_{i=1}^{N} \sum_{j=1}^{N} \langle \mathbf{R}_i \cdot \mathbf{R}_j \rangle = Na^2 \tag{7.14}$$

where a is the segment length: $a = |\mathbf{R}_i|$. The center of mass of the coil is

$$\mathbf{R}_c = \frac{1}{N} \sum_{i=1}^{N} \mathbf{R}_i, \tag{7.15}$$

and the radius of gyration, R_g, is by definition given as

$$R_g^2 = \frac{1}{N} \sum_{i=1}^{N} \langle (\mathbf{R}_i - \mathbf{R}_c)^2 \rangle \tag{7.16}$$

which with Eq. (7.15) inserted gives

$$R_g^2 = \frac{1}{2N^2} \sum_{i=1}^{N} \sum_{j=1}^{N} \langle (\mathbf{R}_i - \mathbf{R}_j)^2 \rangle \tag{7.17}$$

Gaussian polymer coils obey the relation (see e.g., Doi, [1])

$$\langle (\mathbf{R}_j - \mathbf{R}_i)^2 \rangle = a^2 |j - i| \tag{7.18}$$

The radius of gyration is therefore

$$R_g^2 = \frac{1}{2N^2} \sum_{i=1}^{N} \sum_{j=1}^{N} |j - i| a^2 \tag{7.19}$$

For large N we may replace the sum with integrals, getting

$$R_g^2 = \frac{a^2}{2N^2} \int_0^N \int_0^N |j - i| dj\, di = \frac{1}{6} Na^2 = \frac{1}{6} \langle R_\circ^2 \rangle \tag{7.20}$$

Gaussian chains are characterized by the distribution function of the two segments separated by n segments (see e.g., Ref. [1]):

$$P(\mathbf{r}, n) = \left(\frac{3}{2\pi n a^2} \right)^{3/2} \exp\left[-\frac{3\mathbf{r}^2}{2na^2} \right] \tag{7.21}$$

Inserting this into the expression for the correlation function in the scattering function, we get the *form factor* of a Gaussian polymer chain equal the Debye function, g_D:

$$P(\mathbf{q}) = g_D(\mathbf{q}, R_g) = \frac{2}{x^2} (e^{-x} - 1 + x), \quad x = R_g^2 q^2 \tag{7.22}$$

7.3
Thermodynamics of Polymer Blends and Solutions. Flory–Huggins Theory

The phase behavior of polymer blends and solutions is, like any other mixtures, governed by enthalpic interactions between the different units and entropic effects, as described in thermodynamics [1]. The stable phase is determined from the minimum in free energy.

Flory and Huggins proposed a simple theory to calculate the free energy [2]. This theory will be presented based on the lattice model, assuming that polymer segments all occupy equal unit volume (see Figure 7.6). Assume that we have an ensemble of Ω lattice sites available, of which n_A of the polymer chains are A coils, each characterized having N_A segments, that is, a volume fraction equal $\phi_A = n_A N_A/\Omega$. Correspondingly, there are n_B coils of polymer B, each with N_B segments, corresponding to a volume fraction $\phi_B = n_B N_B/\Omega$. Note that an incompressible material is assumed, corresponding to $\phi_A + \phi_B = 1$. The partition function of the system is given by

$$\mathcal{Z} = \sum_i \exp[-E_i/k_B T], \tag{7.23}$$

where E_i is the energy associated to a given configuration, i, of the A- and B-polymers. In the Flory–Huggins model, $\mathcal{Z}$ is calculated in a *mean-field approach* where the site-dependent energy E_i is replaced with a mean value $\bar{E}$, and the number of configurations available for respectively the n_A and the n_B polymer chains are taken into account by a prefactor W. The partition function $\mathcal{Z}$ then becomes

$$\mathcal{Z} \simeq W \exp(-\bar{E}/k_B T) \tag{7.24}$$

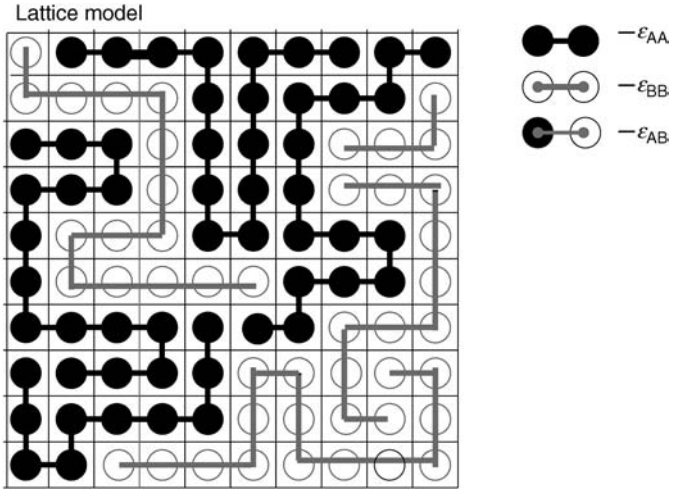

Figure 7.6 The lattice model for a polymer blend.

With the Helmholtz free energy

$$F = -k_B T \ln(\mathcal{Z}) = -TS + U, \tag{7.25}$$

where S is the entropy and U the enthalpy; we thus get the result

$$F = -k_B T \ln(W) + \bar{E} \tag{7.26}$$

It can be seen thereby that W represents the entropy of the system: $k_B \ln W = S$, while $\bar{E}$ is the enthalpic energy.

The average energy in the mixed state is calculated based on the average number of neighboring sites of respectively A and B segments (see Figure 7.6). The enthalpic interaction energy associated with these pairs will be denoted respectively -ε_{AA}, -ε_{BB} and -ε_{AB}. The average energy $\bar{E}$ can then be written as

$$\bar{E}_{\text{mixed}} = -\Omega z \left[\frac{1}{2} \varepsilon_{AA} \phi_{\text{A}}^2 + \frac{1}{2} \varepsilon_{BB} \phi_{\text{B}}^2 + \varepsilon_{AB} \phi_{\text{A}} \phi_{\text{B}} \right] \tag{7.27}$$

where z is the number of nearest neighbors. The corresponding energy of the demixed state is the simple sum of the ε_{AA}-energy of the $\phi_{\text{A}}\Omega_{\text{A}}$-sites and ε_{BB}-energies of the $\phi_{\text{B}}\Omega_{\text{B}}$-sites,

$$\bar{E}_{\text{demixed}} = -\Omega z (\phi_{\text{A}} \varepsilon_{AA}/2 + \phi_{\text{B}} \varepsilon_{BB}/2). \tag{7.28}$$

The change in average enthalpic energy upon mixing is thereby

$$\Delta \bar{E} = \bar{E}_{\text{mixed}} - \bar{E}_{\text{demixed}} = \chi \, \phi_{\text{A}} \phi_{\text{B}} \, k_B T \tag{7.29}$$

where we have used that $\phi_{\text{B}} = 1 - \phi_{\text{A}}$ and where χ is the Flory–Huggins interaction parameter

$$\chi \equiv -\frac{1}{k_B T} \frac{z}{2} (\varepsilon_{AA} + \varepsilon_{BB} - 2\varepsilon_{AB}) \tag{7.30}$$

The ensemble configuration term W, and thereby the entropy, is calculated assuming that each chain can be placed randomly on the lattice, independent of each other. In the homogeneous state, each polymer chain has then

$$w_{\text{A}}(\text{mixed}) = w_{\text{B}}(\text{mixed}) = \Omega \tag{7.31}$$

possible positions of center of mass (translational states), while in the demixed state, the A- and B-polymers have respectively

$$w_{\text{A}}(\text{demixed}) = N_{\text{A}} n_{\text{A}} = \phi_{\text{A}} \Omega \quad \text{and} \quad w_{\text{B}}(\text{demixed}) = N_{\text{B}} n_{\text{B}} = \phi_{\text{B}} \Omega \tag{7.32}$$

possible states. The entropy change by mixing, $\Delta s = k_{\text{B}} \ln w(\text{mixed}) - k_{\text{B}} \ln w(\text{demixed})$ is thus

$$\Delta s_{\text{i}} = k_{\text{B}} \ln(\Omega) - k_{\text{B}} \ln(\phi_{\text{i}} \Omega) = -k_{\text{B}} \ln \phi_{\text{i}}, \quad \text{i} = \text{A or B} \tag{7.33}$$

for each of the two polymer systems. Since the volume fractions are less than 1, Eq. (7.33) tells us that the entropy change Δs_{A} and Δs_{B} upon mixing is always positive; that is, the entropy term of the free energy drag the system toward mixing. To calculate the total entropy of mixing, $\Delta \tilde{S}$, the entropy contribution from

each polymer molecule Δs_A and Δs_B is summed:

$$\Delta \tilde{S}_{mix} = n_A \Delta s_A + n_B \Delta s_B = -k_B n_A \ln \phi_A - k_B n_B \ln \phi_B \tag{7.34}$$

Substituting $n_A = \phi_A \Omega / N_A$ and $n_B = \phi_A \Omega / N_A$, and dividing by the number of lattice sites, we get the change of entropy per unit volume:

$$\Delta S_{mix} = -k_B \left[\frac{\phi_A}{N_A} \ln \phi_A + \frac{\phi_B}{N_B} \ln \phi_B \right] \tag{7.35}$$

The Helmholtz free energy of mixing is the sum of entropic and enthalpic contribution according to

$$F_m = -T\Delta S + \Delta \bar{E} \tag{7.36}$$

which, using Eqs (7.29) and (7.35), is rewritten into the Flory–Huggins formula

$$F_m(\phi) = k_B T \left[\frac{\phi_A}{N_A} \ln \phi_A + \frac{\phi_B}{N_B} \ln \phi_B + \chi \phi_A \phi_B \right] \tag{7.37}$$

For classical, low-molar-mass liquids (corresponding to N_A and N_B equal to 1 in Eq. (7.37)), the driving force for mixing is typically the gain in entropy. For polymer blends, the large molecular sizes (large N-values) markedly reduce the entropic gain. The result is the general statement, that typical polymers do not mix. Only when the enthalpic forces under special circumstances effectively becomes very small, will the entropy cause polymers to mix.

Whether a system of two polymers, A and B remains phase-separated or will mix can be predicted from the ϕ dependence of the free energy function, $F_m(\phi)$. Suppose that the free energy function F_m has a U-shaped ϕ-dependence, and consider a sample with polymer A concentration equal to ϕ. If the blend tend to demix into concentrations ϕ_1 and ϕ_2 it will have the free energy, F_{demix}, this being the concentration-weighted average of the energies in the two concentrations ϕ_1 and ϕ_2. With the U-shaped ϕ-dependence of F_m, the demixed energy will be larger than the mixed, and the system equilibrium is in the mixed state. If the ϕ-dependence of the free energy of mixing F_m, on the other hand is $\cap$-shaped, the free energy of the phase separated state is lower than that of the mixed, and the thermodynamic stable state is phase separated. Thermodynamically, the free energy has a U-shaped ϕ-dependence of F_m nearby the two *binodal* points (*B*1 and *B*2), which can be shown to fulfill the relation

$$\left. \frac{\partial F_m}{\partial \phi} \right|_{\phi_{B1}} = \left. \frac{\partial F_m}{\partial \phi} \right|_{\phi_{B2}} \tag{7.38}$$

Thus, for phase-separated systems, the concentrations ϕ_{B1} and ϕ_{B2} of the two thermodynamic stable phases are uniquely determined by the points of common tangent. The inflection points separating U- from I-shaped $F(\phi)$ will accordingly represent an *instability* points, the so-called *spinodal points* given by the condition

$$\left. \frac{\partial^2 F_m}{\partial \phi^2} \right|_{\phi_{S1}} = \left. \frac{\partial^2 F_m}{\partial \phi^2} \right|_{\phi_{S2}} = 0 \tag{7.39}$$

Systems with concentrations between the two spinodal points will be unstable and decompose spontaneously. Polymer mixtures with overall concentrations between the binodal and the spinodal, will be metastable, and decompose following a nucleation-and-growth mechanism. For polymer blends with concentrations "outside" the two binodals, the system is mixed in a thermodynamically stable single phase.

The free energy function depends generally on temperature – that is, the binodal and spinodal concentrations varies on changing temperature. At a given temperature, the two binodals and the two spinodals all meet at one point in the concentration–temperature phase-diagram. This is the *critical point* given by

$$\frac{\partial^3 F_m}{\partial \phi^3} = 0 \tag{7.40}$$

For a symmetric polymer blend, $N_A = N_B = N$, the equations above lead to a critical point given by relation

$$\chi_c N = 2 \tag{7.41}$$

7.4 The Scattering Function and Thermodynamics

In the preceding chapter we have, based on the Flory–Huggins theory, discussed the basis for the phase behavior of polymer blends. Miscible polymer blends and polymer solutions have, even in the mixed one-phase system, spatial variations in the polymer concentration. These *concentration fluctuations* reflect the thermodynamic parameters of the free energy, as described in the Flory–Huggins model.

In a real polymer material, the fluctuations are not limited to chemical composition fluctuations. Thermal density fluctuations will generally also be present and can be measured. According to the fluctuation–dissipation theorem, these fluctuations are characterized by the material compressibility $\partial \ln V/\partial P$, where V is the volume and P the pressure [3]. In neutron scattering experiments using labeled chains (see Figure 7.3), the thermal fluctuations are negligible as compared to composition fluctuations. We will, for simplicity, neglect thermal density fluctuations and assume a constant segment density, that is, in the lattice model (Figure 7.6) we assume that every lattice site is filled with polymer *segments* imposed by the constraint

$$\phi_A(\mathbf{R}) + \phi_B(\mathbf{R}) = 1 \tag{7.42}$$

satisfied for all sites $\mathbf{R}$. The concentration fluctuations can be measured directly by scattering methods; hence, scattering experiments can provide insight into the thermodynamics of polymer systems.

The ensemble-averaged concentrations $\phi_A = \langle \phi_A(\mathbf{R}) \rangle$ and $\phi_B = \langle \phi_B(\mathbf{R}) \rangle$ must fulfill the same relation $\phi_A + \phi_B = 1$. The fluctuation terms are advantageously described by the deviation of the segment density from average at each lattice site;

rather than the concentrations themselves:

$$\begin{aligned}\delta\phi_A(\mathbf{R}) &= \phi_A(\mathbf{R}) - \phi_A \\ \delta\phi_B(\mathbf{R}) &= \phi_B(\mathbf{R}) - \phi_B\end{aligned} \tag{7.43}$$

With the density constraint the fluctuation $\delta\phi_A$ and $\delta\phi_B$ terms holds:

$$\delta\phi_A(\mathbf{R}) + \delta\phi_B(\mathbf{R}) = 0 \tag{7.44}$$

The product

$$\delta\phi_i(\mathbf{R})\delta\phi_j(\mathbf{R}+r) \quad i = A, B; \quad j = A, B. \tag{7.45}$$

characterizing the spatially correlated fluctuations is a unique measure of the thermodynamics. Equation (7.45) describes the correlation between segments i in a position $\mathbf{R}$ with those of species j in position $\mathbf{R} + \mathbf{r}$.

Usually, these correlations would be expect to have a relatively short range, since distant segments will be completely independent. The products in Eq. (7.45) will accordingly be nonzero only for relatively small values of $\mathbf{r}$.

The thermodynamics of the system is described in terms of the ensemble average, $\gamma_{ij}(\mathbf{r})$, of the spatially correlated fluctuations:

$$\gamma_{ij}(\mathbf{r}) = \langle\delta\phi_i(\mathbf{R})\delta\phi_j(\mathbf{R}+\mathbf{r})\rangle \quad i = A, B; \quad j = A, B. \tag{7.46}$$

where $\langle\cdots\rangle$ denotes the ensemble average. With $\delta\phi_A = -\delta\phi_B$, it follows that

$$\gamma_{AA}(\mathbf{r}) = \gamma_{BB}(\mathbf{r}) = -\gamma_{AB}(\mathbf{r}) = -\gamma_{BA}(\mathbf{r}), \tag{7.47}$$

which leads to the important and very simple result: The concentration fluctuations of an incompressible two component system are characterized by a *single correlation function* $\gamma(\mathbf{r})$ which, by definition, will be associated with the self-correlation function:

$$\gamma(\mathbf{r}) \equiv \gamma_{AA}(\mathbf{r}). \tag{7.48}$$

The correlation function is, as mentioned above, tightly related to the thermodynamics of the system. Furthermore, the Fourier transform of the spatial correlation functions can be measured directly in neutron scattering experiments, as outlined in Eq. (7.12). This will be discussed further below.

7.4.1 The Forward Scattering

The experimentally accessible correlation function, $\gamma_{ij}(\mathbf{r}) = \langle\phi_i(\mathbf{R})\phi_j(\mathbf{R}+\mathbf{r})\rangle$, can be expressed in terms of thermodynamic parameters. In order to calculate the correlation functions $\gamma_{ij}(\mathbf{r})$, we follow basically the route of de Gennes [4] and Doi [1], using the fact that the correlation function can be shown to express the proportionality constant when using *linear response theory* to treat energy changes.

To find the thermodynamic relationship to the correlation function, we start to calculate the response on the total energy upon perturbating individual segments with a weak external potential. Let us assume that the potentials $u_A(\mathbf{R})$ and $u_B(\mathbf{R})$

act on, respectively, A and B segments in site **R**. The resulting change in the system's potential energy is then

$$U_e = \int [u_A(\mathbf{R})\phi_A(\mathbf{R}) + u_B(\mathbf{R})\phi_B(\mathbf{R})]d\mathbf{R} \tag{7.49}$$

where the subscript e denotes "external" and where we have used a continuous description of the ensemble ($\int_{\mathbf{R}}$) rather than the lattice representation ($\sum_{\mathbf{R}}$). The u_A and u_B external potentials acting on individual sites will cause local deviation from average composition; that is, generally we may expect that $\phi_A(\mathbf{R})$ is not equal to ϕ_A and $\phi_B(\mathbf{R})$ is not equal to ϕ_B. With $U_\circ$ being the intrinsic energy of the system, the equilibrium average can be written as

$$\overline{\delta\phi_A}(\mathbf{R}) = \frac{\int \delta\phi_A(\mathbf{R})\exp[-(U_\circ + U_e)/(k_BT)]d\mathbf{r}}{\int \exp[-(U_\circ + U_e)/k_BT]d\mathbf{r}} \tag{7.50}$$

according to statistical mechanics ([5]). We rewrite the formula into the form

$$\overline{\delta\phi_A}(\mathbf{R}) = \frac{\langle \delta\phi_A(\mathbf{R})\exp[-U_e/(k_BT)]\rangle}{\langle \exp[-U_e/(k_BT)]\rangle} \tag{7.51}$$

where $\langle\cdots\rangle \equiv \int(\cdots)e^{-U_\circ/k_BT}d\mathbf{r}/\int e^{-U_\circ/k_BT}d\mathbf{r}$ denotes the equilibrium average without external fields. For weak external fields, $U_e/k_BT \ll 1$ we can make the approximations

$$\exp(-U_e/(k_BT) \approx 1 - U_e/(k_BT) \quad \text{and} \quad \frac{1}{1 - U_e/(k_BT)} \approx 1 + U_e/(k_BT)$$

making Eq. (7.51) into the form

$$\overline{\delta\phi_A}(\mathbf{R}) \approx \langle \delta\phi_A(\mathbf{R})\rangle(1 + \langle U_e/k_BT\rangle) - \langle \delta\phi_A U_e/k_BT\rangle \tag{7.52}$$

to first order in $U_e/(k_BT)$. The first term in Eq. (7.52) vanishes, as the equilibrium average of $\delta\phi_A(\mathbf{R})$ by definition is zero without external fields. With Eq. (7.49) it thus follows from Eq. (7.52) that

$$\overline{\delta\phi_A}(\mathbf{R}) \approx -\frac{1}{k_BT}\langle \delta\phi_A(\mathbf{R})\, U_e\rangle$$

which, when using the expression for $U_\circ$ can be rewritten into

$$\begin{aligned}\overline{\delta\phi_A}(\mathbf{R}) \approx -\frac{1}{k_BT}\langle \delta\phi_A(\mathbf{R}) \int [\phi_A u_A(\mathbf{R}+\mathbf{r}) + \phi_B u_B(\mathbf{R}+\mathbf{r})]d\mathbf{r} + \\ \delta\phi_A(\mathbf{R}) \int [\delta\phi_A(\mathbf{R}+\mathbf{r})u_A(\mathbf{R}+\mathbf{r}) + \delta\phi_B(\mathbf{R}+\mathbf{r})u_B(\mathbf{R}+\mathbf{r})]d(\mathbf{R}+\mathbf{r})\rangle\end{aligned} \tag{7.53}$$

Assuming that the potentials $u_A(\mathbf{R})$ and $u_B(\mathbf{R})$ varies little over the length scale of fluctuations, the first term vanished due to mean zero of $\delta\phi_A(\mathbf{R})$. The fluctuation term then becomes

$$\begin{aligned}\overline{\delta\phi_A}(\mathbf{R}) = -\frac{1}{k_BT}\Big[\int \langle \delta\phi_A(\mathbf{R})\delta\phi_A(\mathbf{R}+\mathbf{r})\rangle u_A(\mathbf{R}+\mathbf{r})d\mathbf{r} + \\ \int \langle \delta\phi_A(\mathbf{R})\delta\phi_B(\mathbf{R}+\mathbf{r})\rangle u_B(\mathbf{R}+\mathbf{r})d\mathbf{r}\Big]\end{aligned} \tag{7.54}$$

The result Eq. (7.54), originally derived by de Gennes [4], is most important. It expresses the *linear response theory* that the thermal averaged local concentration fluctuations depends linearly on the fields acting on any other sites, with proportionality constants equal the spatial correlation functions $\gamma_{AA}(\mathbf{r})$ and $\gamma_{AB}(\mathbf{r})$, as defined in Eq. (7.46). Using further that $\delta\phi_B(\mathbf{R}) = -\delta\phi_A(\mathbf{R})$, Eq. (7.54) may be rewritten into

$$\begin{aligned}\overline{\delta\phi_A}(\mathbf{R}) &= -\frac{1}{k_B T}\int \langle \delta\phi_A(\mathbf{R})\delta\phi_A(\mathbf{R}+\mathbf{r})\rangle [u_A(\mathbf{R}+\mathbf{r}) - u_B(\mathbf{R}+\mathbf{r})]d\mathbf{r} \\ &= -\frac{1}{k_B T}\int \gamma(\mathbf{r})[u_A(\mathbf{R}+\mathbf{r}) - u_B(\mathbf{R}+\mathbf{r})]d\mathbf{r}\end{aligned} \tag{7.55}$$

where the definition Eq. (7.48), $\gamma \equiv \gamma_{AA}$, is used.

The correlation function γ is expected to be of relative short range, that is, γ is likely non-zero only for **r**-values up to some coil-diameters in the mixed phase. We will therefore, as above, assume that the spatial variation of $u_A(\mathbf{R})$, $u_B(\mathbf{R})$ is gradual, so that these potentials can be considered constant over the range where $\gamma(\mathbf{r})$ has a nonzero value. In this case, Eq. (7.55) can be approximated as follows

$$\overline{\delta\phi_A}(\mathbf{R}) \simeq -\frac{1}{k_B T}[u_A(\mathbf{R}) - u_B(\mathbf{R})]\int \gamma(\mathbf{r})d\mathbf{r} \tag{7.56}$$

The Fourier transform of $\gamma(\mathbf{r})$ is the structure factor $I(\mathbf{q})$ (Eq. (7.12)) given by

$$I(\mathbf{q}) = \int \gamma(\mathbf{r})\exp[-i\mathbf{q}\cdot\mathbf{r}]d\mathbf{r}. \tag{7.57}$$

The integral in Eq. (7.56) can thereby be expressed in terms of the structure factor at zero **q**-value, that is,

$$\overline{\delta\phi_A}(\mathbf{R}) = -\frac{1}{k_B T} I(0)[u_A(\mathbf{R}) - u_B(\mathbf{R})] \tag{7.58}$$

With $u_A(\mathbf{R})$ and $u_B(\mathbf{R})$ assumed to be almost constant, the deviation $\overline{\delta\phi_A}(\mathbf{R})$ is determined from the condition of thermodynamic equilibrium as expressed by the chemical potentials μ_A and μ_B. In the absence of external fields, we have, according to thermodynamics:

$$\left(\frac{\partial F_m}{\partial \phi}\right)\Big|_{\mathbf{r}} + [\mu_A(\mathbf{r}) - \mu_B(\mathbf{r})] = C \tag{7.59}$$

where C is a constant independent of concentration. With perturbations with the small external potentials, $u_A(\mathbf{R})$ and $u_B(\mathbf{R})$, the local chemical potentials $\mu_A(\mathbf{R})$ and $\mu_B(\mathbf{R})$ will change by these respective values. The changes in the free-energy derivative is expressed in terms of the associated change in concentration

$$\Delta\left(\frac{\partial F_m}{\partial \phi}\right)\Big|_{\mathbf{R}} \simeq \left(\frac{\partial^2 F_m}{\partial \phi^2}\right)\Big|_{\mathbf{R}} \overline{\delta\phi}(\mathbf{R}) \tag{7.60}$$

assuming that the fluctuation-term $\overline{\delta\phi}(\mathbf{R})$ is small. From these perturbations in respectively free energy and chemical potential, Eq. (7.59) thereby gives the

condition for thermodynamic equilibrium

$$\left(\frac{\partial^2 F_m}{\partial \phi^2}\right)\overline{\delta\phi}(\mathbf{R}) + [u_A(\mathbf{R}) - u_B(\mathbf{R})] = 0 \tag{7.61}$$

and thereby

$$\overline{\delta\phi}(\mathbf{R}) = -\left(\frac{\partial^2 F_m}{\partial \phi^2}\right)^{-1}[u_A(\mathbf{R}) - u_B(\mathbf{R})] \tag{7.62}$$

Combining Eq. (7.62) with Eq. (7.58) describes thereby the fluctuation correlation function in terms of thermodynamics

$$I(0) = \int \gamma(\mathbf{r})d\mathbf{r} = k_B T\left(\frac{\partial^2 F_m}{\partial \phi^2}\right)^{-1}, \tag{7.63}$$

that is, the structure factor, $I(0)$, is directly related to the thermodynamics of the polymer blend. The spinodal point of polymer blends, $\partial^2 F_m/\partial\phi^2 = 0$, can thus be obtained experimentally by measuring the structure factor at $\mathbf{q} = 0$, and extract the temperature where the $I^{-1}(\mathbf{0})$ approach zero (see Figure 7.7).

Figure 7.7 shows an experimental example of such studies, showing the forward scattering $I(0)$ of a polymer blend of polystyrene (PS) and poly(vinylmethylether) (PVME) with a given concentration ($\phi_{PS} = 0.32$) [6]. The forward scattering is obtained from experimental $I(q)$ data extrapolating $q \to 0$. A number of equivalent data, obtained for various concentrations, may give the whole spinodal curve.

The coexistence curve, or the binodal, can also be obtained from the same scattering experiments, identifying the abrupt and (usually, due to the relative slow

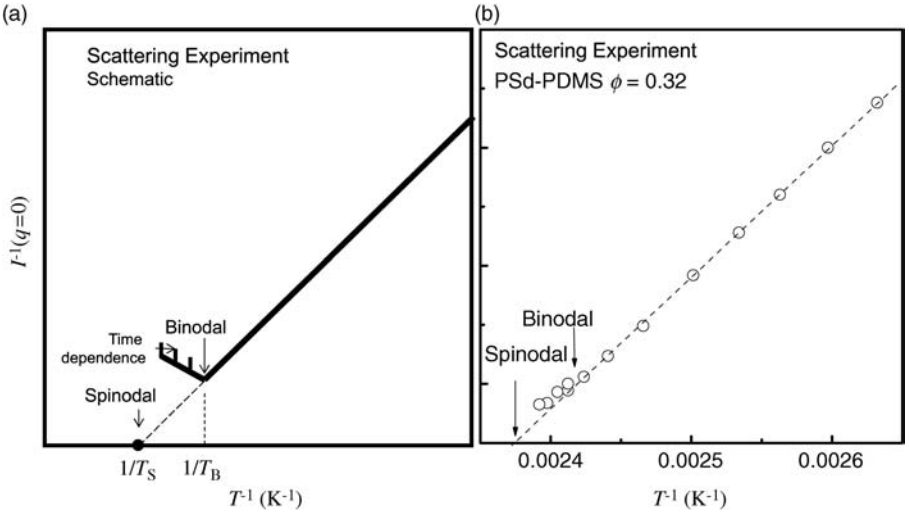

Figure 7.7 Small-angle neutron scattering data $I^{-1}(0)$ versus T^{-1} identifying the spinodal and the binodal temperatures. (a) $I^{-1}(0)$ versus T^{-1} schematically; (b) An experimental example of a polymer blend of polystyrene (PS) and poly(vinyl methylether) (PVME) giving the experimental spinodal and binodal values. The linear $I^{-1}(0)$ versus T^{-1} is in accordance with the RPA result (Eq. (7.82)), with $\chi \propto T^{-1}$. Experimental data reproduced from Ref. [6].

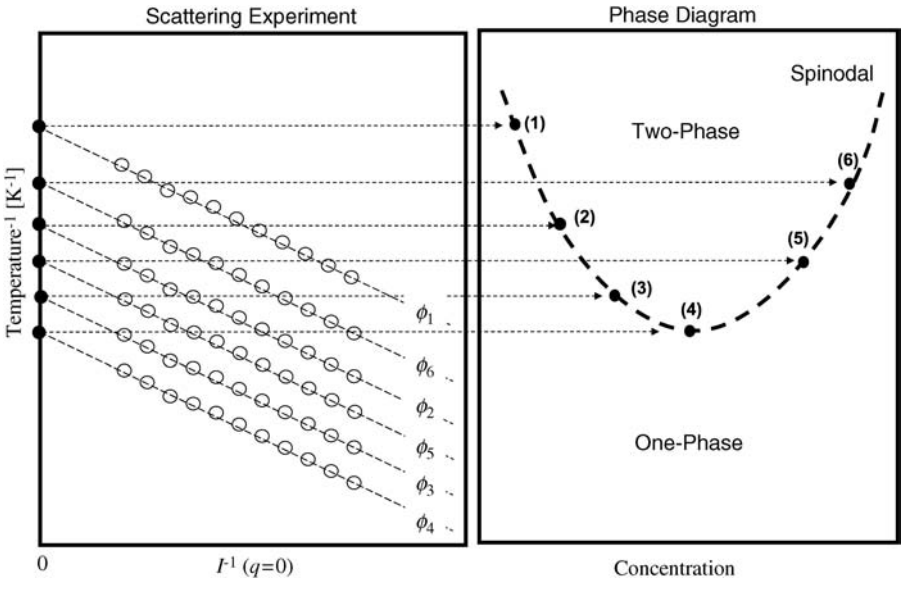

Figure 7.8 By measuring the forward scattering $I(\mathbf{q} = 0)$ it is possible experimentally to determine the spinodal curve (second derivative of free energy, $\partial^2 F_m/\partial\phi^2$, is zero) of the binary phase diagram, since $\partial^2 F_m/\partial\phi^2 = I^{-1}(0)$.

nucleation and growth mechanism) time-dependent deviation in the I^{-1} versus T^{-1} plot (T_B in the Figure 7.7).

By measuring the temperature dependence of $I(0)$ for a variety of concentrations, as sketched in Figure 7.8, the spinodal phase boundary can be mapped out for polymer blends.

7.4.2
Random Phase Approximation (RPA)

In the next section, an attempt will be made to evaluate further details on the composition fluctuations as related to the experimental scattering function, $I(\mathbf{q})$.

The calculations will be based on the result (see Eq. (7.55)) that the pair correlation function is expressed in terms of linear response theory. The calculations will further be made using a mean-field approximation principally where the excluded volume effects, the density constrain and the interactions between chains are taken into account as perturbations, expressed in terms of potential energies. This calculation is called the random phase approximation (RPA).

Initially, consider the case where polymers A and B are placed on the lattice at random, without any excluded volume effects or interaction energies. In this case, there is by definition no correlation in the positioning of polymers segments A and B, and the correlation term $\langle \delta\phi_A(\mathbf{R})\delta\phi_B(\mathbf{R}+\mathbf{r})\rangle$ obviously equals zero. The correlations $\langle \delta\phi_A(\mathbf{R})\delta\phi_A(\mathbf{R}+\mathbf{r})\rangle$ and $\langle \delta\phi_B(\mathbf{R})\delta\phi_B(\mathbf{R}+\mathbf{r})\rangle$ between A − A and B − B

segments, on the other hand, are both finite since the segments of the polymers are linked together making up A and B polymer chains, respectively. If external fields $u_A(\mathbf{R})$ and $u_B(\mathbf{R})$ are applied to this system, the resulting change in the concentration $\overline{\delta\phi_A}(\mathbf{R})$ is then responding with the change in fluctuations (Eq. (7.54))

$$\overline{\delta\phi_A}(\mathbf{R}) = -\frac{1}{k_B T}\int \gamma^{\circ}_{AA}(\mathbf{r}) u_A(\mathbf{R}+\mathbf{r}) d\mathbf{r} \tag{7.64}$$

where the response function is identical to the pair correlation function, as discussed above in Eq. (7.55). Now, in reality there are of course both enthalpic interactions between the chains and volume constraint. These terms will be taken into account as perturbations using a mean field approximation.

If the concentrations of A and B segments in position $\mathbf{R}$ are respectively $\overline{\phi_A}(\mathbf{R}) = \phi_A + \overline{\delta\phi_A}(\mathbf{R})$ and $\overline{\phi_B}(\mathbf{R}) = \phi_B + \overline{\delta\phi_B}(\mathbf{R})$, the enthalpic fields acting on the segments A and B are given by respectively,

$$\begin{aligned} w_A(\mathbf{R}) &= -z[\varepsilon_{AA}\overline{\phi_A}(\mathbf{R}) + \varepsilon_{AB}\overline{\phi_B}(\mathbf{R})] \qquad \text{and} \\ w_B(\mathbf{R}) &= -z[\varepsilon_{BA}\overline{\phi_A}(\mathbf{R}) + \varepsilon_{BB}\overline{\phi_B}(\mathbf{R})] \end{aligned} \tag{7.65}$$

The conservation of volume condition: $\phi_A(\mathbf{R}) + \phi_B(\mathbf{R}) = 1$, will thermodynamically correspond to a force acting on each site, expressed as a potential, $V(\mathbf{R})$. The total energy U_{excl} representing the excluded volume effect is then calculated by integrating $V(\mathbf{R})$ over volume:

$$U_{excl} \equiv \int V(\mathbf{R}) d\mathbf{R} = \int V(\mathbf{R})[\phi_A(\mathbf{R}) + \phi_B(\mathbf{R})] d\mathbf{R} \tag{7.66}$$

where in the last equality we have replaced a factor 1 with the identical $[\phi_A(\mathbf{R}) + \phi_B(\mathbf{R})]$ sum. The internal fields acting on segments A and B are the sums, respectively $w_A + V$ and $w_B + V$. In the linear response theory $\overline{\delta\phi_A}$ and $\overline{\delta\phi_B}$ can thus be expressed as

$$\overline{\delta\phi_A}(\mathbf{R}) = \frac{1}{k_B T}\int \gamma^{\circ}_{AA}(\mathbf{R})[u_A(\mathbf{R}+\mathbf{r}) + w_A(\mathbf{R}+\mathbf{r}) + V(\mathbf{R}+\mathbf{r})] d\mathbf{r} \tag{7.67}$$

$$\overline{\delta\phi_B}(\mathbf{R}) = \frac{1}{k_B T}\int \gamma^{\circ}_{BB}(\mathbf{R})[u_B(\mathbf{R}+\mathbf{r}) + w_B(\mathbf{R}+\mathbf{r}) + V(\mathbf{R}+\mathbf{r})] d\mathbf{r} \tag{7.68}$$

The constraint $\phi_A(\mathbf{R}) + \phi_B(\mathbf{R}) = 1$ gives, as discussed already above,

$$\overline{\delta\phi_A}(\mathbf{R}) + \overline{\delta\phi_B}(\mathbf{R}) = 0 \tag{7.69}$$

Equations (7.67)–(7.69) form a set of simultaneous equations for the unknowns $\overline{\delta\phi_A}(\mathbf{R})$, $\overline{\delta\phi_B}(\mathbf{R})$, and $V(\mathbf{R})$. To solve these equations, we will use the Fourier transform of $\delta\phi(\mathbf{R})$ and $V(\mathbf{R})$. In setting the formula Eq. (7.67) for the concentration fluctuation expressed in terms of the spatial correlation function, the Fourier transformed $\overline{\delta\phi}(\mathbf{R})$ acquires the form

$$\begin{aligned} \overline{\delta\psi_A}(\mathbf{q}) &= \frac{1}{V}\int \overline{\delta\phi_A}(\mathbf{r}) \exp[i\mathbf{q}\cdot\mathbf{r}] d\mathbf{r} \\ &\simeq -\frac{1}{V}\frac{1}{k_B T}[u_A - u_B]\int\int \gamma(\mathbf{r}) \exp[i\mathbf{q}\cdot\mathbf{r}] d\mathbf{R} \quad d\mathbf{r} \\ &= -\frac{1}{k_B T} I(\mathbf{q})[u_A - u_B], \end{aligned} \tag{7.70}$$

where we used the formula for the structure factor, $I(\mathbf{q})$ (Eq. (7.12)).

After some mathematical rewritings, using the expression for the unperturbed structure factor of noninteracting polymer chains

$$I^{\circ}_{AA}(\mathbf{q}) = \int \gamma^{\circ}_{AA}(\mathbf{r}) e^{-i\mathbf{q}\cdot\mathbf{r}} d\mathbf{r}, \tag{7.71}$$

that $w_{\mathrm{A}}(\mathbf{R}) = -z[\varepsilon_{AA}\overline{\phi}_{\mathrm{A}}(\mathbf{R}) + \varepsilon_{AB}\overline{\phi}_{\mathrm{B}}(\mathbf{R})]$, and that $\vartheta(\mathbf{q})$ is the Fourier transform of the potential $V(\mathbf{R})$, we find

$$\overline{\delta\psi_{\mathrm{A}}}(\mathbf{q}) = -\frac{1}{k_B T} I^{\circ}_{\mathrm{AA}}(\mathbf{q}) \left[u_{\mathrm{A}} - z\left[\varepsilon_{\mathrm{AA}}\overline{\delta\psi_{\mathrm{A}}}(\mathbf{q}) + \varepsilon_{\mathrm{AB}}\overline{\delta\psi_{\mathrm{B}}}(\mathbf{q})\right] + \vartheta(\mathbf{q})\right] \tag{7.72}$$

The corresponding expression for the Fourier transform $\overline{\delta\psi_{\mathrm{B}}}(\mathbf{q})$ of $\overline{\delta\phi_{\mathrm{B}}}(\mathbf{r})$ is

$$\overline{\delta\psi_{\mathrm{B}}}(\mathbf{q}) = -\frac{1}{k_B T} I^{\circ}_{\mathrm{BB}}(\mathbf{q}) \left[u_{\mathrm{B}} - z\left[\varepsilon_{\mathrm{BA}}\overline{\delta\psi_{\mathrm{A}}}(\mathbf{q}) + \varepsilon_{\mathrm{BB}}\overline{\delta\psi_{\mathrm{B}}}(\mathbf{q})\right] + \vartheta(\mathbf{q})\right] \tag{7.73}$$

The sum, $\overline{\delta\psi_{\mathrm{A}}}(\mathbf{q}) + \overline{\delta\psi_{\mathrm{B}}}(\mathbf{q})$, of these two Fourier transforms is zero, according to

$$\overline{\delta\psi_{\mathrm{A}}}(\mathbf{q}) + \overline{\delta\psi_{\mathrm{B}}}(\mathbf{q}) = \int [\overline{\delta\phi_{\mathrm{A}}}(\mathbf{r}) + \overline{\delta\phi_{\mathrm{B}}}(\mathbf{r})] e^{i\mathbf{q}\cdot\mathbf{r}} \quad d\mathbf{r} = 0 \tag{7.74}$$

Solving the three Eqs (7.72)–(7.74) with the three unknowns $\overline{\delta\psi_{\mathrm{A}}}$, $\overline{\delta\psi_{\mathrm{B}}}$ and ϑ give

$$\overline{\delta\psi_{\mathrm{A}}}(\mathbf{q}) = -\frac{1}{k_B T}\left[\frac{1}{I^{\circ}_{\mathrm{AA}}(\mathbf{q})} + \frac{1}{I^{\circ}_{\mathrm{BB}}(\mathbf{q})} - 2\chi\right]^{-1} (u_{\mathrm{A}} - u_{\mathrm{B}}) \tag{7.75}$$

Here, $\chi = z/(2k_B T)[\varepsilon_{\mathrm{AA}} + \varepsilon_{\mathrm{BB}} - 2\varepsilon_{\mathrm{AB}}]$ is the Flory–Huggins interaction parameter defined above (Eq. (7.30)). From Eq. (7.70) the structure factor $I(\mathbf{q})$ is thereby given by the rather simple expression

$$\frac{1}{I(\mathbf{q})} = \frac{1}{I^{\circ}_{\mathrm{AA}}(\mathbf{q})} + \frac{1}{I^{\circ}_{\mathrm{BB}}(\mathbf{q})} - 2\chi \tag{7.76}$$

Equation (7.76) may be rewritten into the more general RPA form,

$$I(\mathbf{q}) = \frac{N}{F_{\mathrm{blend}}(\mathbf{q}) - 2\chi N} \tag{7.77}$$

where the function $F(\mathbf{q})$ for blends is given by

$$F_{\mathrm{blend}}(\mathbf{q}) = \frac{1}{N}\left[\frac{1}{I^{\circ}_{\mathrm{AA}}(\mathbf{q})} + \frac{1}{I^{\circ}_{\mathrm{BB}}(\mathbf{q})}\right] = \frac{1}{N}\frac{I^{\circ}_{\mathrm{AA}}(\mathbf{q}) + I^{\circ}_{\mathrm{BB}}(\mathbf{q})}{I^{\circ}_{\mathrm{AA}}(\mathbf{q}) I^{\circ}_{\mathrm{BB}}(\mathbf{q})} \tag{7.78}$$

with the "average" degree of polymerization, N, defined as

$$N = \frac{N_{\mathrm{A}} N_{\mathrm{B}}}{N_{\mathrm{A}} + N_{\mathrm{B}}} \tag{7.79}$$

The individual polymer coils obey Gaussian statistics with the associated Debye-function (Eq. (7.22)) giving the bare structure factors, that is,

$$I^{\circ}(\mathbf{q}) = \phi N g_D(q, N), \tag{7.80}$$

Using further the approximation

$$g_D(x) = 2/(x^4) \cdot \left[\exp(-x^2) - 1 + x^2\right] \approx 1 - \frac{1}{3}x^2 \approx \frac{1}{1 + \frac{1}{3}x^2} \tag{7.81}$$

the RPA expression, Eq. (7.76) becomes

$$\frac{1}{I(\mathbf{q})} = \frac{1 + q^2 R_{\mathrm{A}}^2/3}{\phi_{\mathrm{A}} N_{\mathrm{A}}} + \frac{1 + q^2 R_{\mathrm{B}}^2/3}{\phi_{\mathrm{B}} N_{\mathrm{B}}} - 2\chi \tag{7.82}$$

which we rewrite into

$$I^{-1}(\mathbf{q}) = \left[\frac{1}{\phi_A N_A} + \frac{1}{\phi_B N_B} - 2\chi\right] + \left[\frac{R_A^2}{3\phi_A N_A} + \frac{R_B^2}{3\phi_B N_B}\right] q^2 \tag{7.83}$$

that is, the scattering function has the simple Lorentzian (Ornstein–Zernike) form:

$$I^{-1}(\mathbf{q}) = I^{-1}(0)[1 + \xi^2 q^2] \tag{7.84}$$

where

$$I^{-1}(0) = \frac{1}{\phi_A N_A} + \frac{1}{\phi_B N_B} - 2\chi \tag{7.85}$$

is the forward scattering already discussed above, relating directly to the thermodynamics of the system. The correlation length ξ

$$\xi = \left[\frac{R_A^2}{3\phi_A N_A} + \frac{R_B^2}{3\phi_B N_B}\right]^{1/2} \sqrt{I(0)} \tag{7.86}$$

describes the spatial extend of the fluctuations. We see that the RPA theory expresses thermodynamic properties of polymer blends, as described within the Flory–Huggins model, in terms of experimental accessible parameters. Measurements of the scattering function as a function of composition and temperatures provide both the spinodal phase boundary, and the temperature and concentration dependent Flory–Huggins interaction parameter (χ). The Flory–Huggins model describes the enthalpic interactions in terms of temperature independent neighboring interactions ε_{ij}, giving a T^{-1}-dependent χ-parameter. The mean field treatment thus predict the following scaling for forward scattering and correlation length:

$$I(0) \propto T^{-1} \quad \text{and} \quad \xi \propto T^{-1/2} \tag{7.87}$$

as already used in Figures 7.7 and 7.8. Figures 7.9 and 7.10 shows experimental scattering functions for two polymer systems: a polystyrene/poly(vinyl

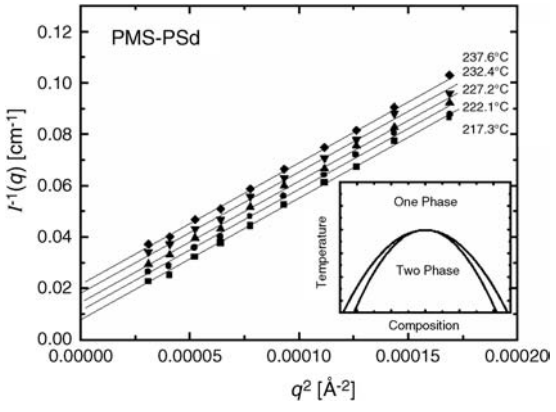

Figure 7.9 Small-angle neutron scattering experiments of polymer blends of polystyrene (PS) and poly(methylstyrene) (PMS) showing the agreement with the RPA-result: $I^{-1}(q)$ linear in q^2. The inset shows schematically the phase diagram, which for the PS/PMS system is of the UCST-type. The PS polymers are deuterated (PSd) in order to obtain contrast between the two polymers in the neutron scattering experiment. Experimental data reproduced from Ref. [7].

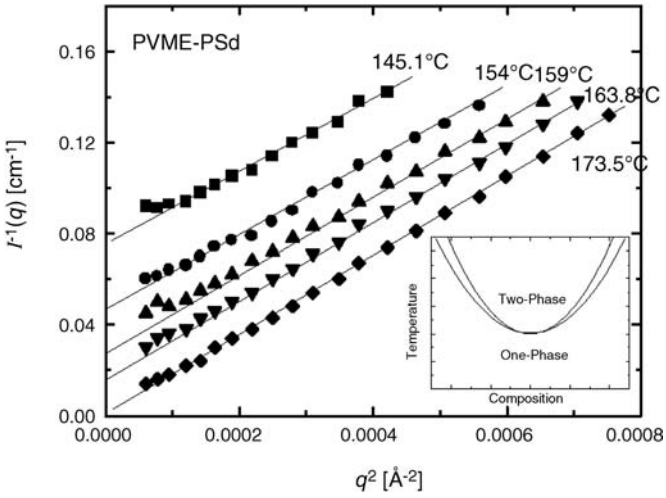

Figure 7.10 Small-angle neutron scattering experiments of polymer blends of polystyrene (PS) and poly(vinylmethylether) (PVME) showing the agreement with the RPA-result: $I^{-1}(q)$ linear in q^2. The insert shows schematically the phase diagram, which for the PS/PVME system is of the LCST-type. The PS polymers are deuterated (PSd) in order to obtain contrast between the two polymers in the neutron scattering experiment. Experimental data reproduced from Ref. [7].

methylether) blend and a polystyrene/poly(methylstyrene) blend, plotted as I^{-1} versus q^2. The results are in agreement with the RPA result Eq. (7.82) and exhibit the expected linear relationships based on Flory–Huggins thermodynamics and mean-field random phase approximation. It may be noted that for the PS/PMS system, the $I^{-1}(0)$-parameter decreases upon lowering the temperature (i.e., $I(0)$ increases) implying that the system is mixed at high temperature and demixed at low temperature, an upper critical solution temperature (UCST) system. The PVME/PS system is opposite, having a lower critical solution temperature (LCST).

The χ-parameter is, according to the definition (Eq. (7.30)), assumed to be purely enthalpic and short-ranged. It reflects segmental nearest neighbor interactions, which are likely to be dominated by dipole–dipole interactions. Experimentally determined χ-values appear to be more complex; only high-molar-mass polymers have effectively a segmental χ-parameter where end-effects are negligible, and the temperature-dependence is seldom pure T^{-1}. In spite of such difficulties, the mean-field random phase approximation and Flory–Huggins theory provide an excellent basis for analyzing polymer thermodynamics.

7.4.3 Beyond Mean Field

The RPA method is based on a completely random organization of the polymer chains where the effects of interactions are estimated using a perturbation calculation. Such mean field calculations are only valid as long as the length scale of the fluctuations are small compared to characteristic lengths of the system (the

Ginzburg criteria). In a region close to the critical point, T_c, thermal composition fluctuations may significantly renormalize the thermodynamics. In polymers, relevant length scales separating valid mean-field from non-mean-field characteristics may be the correlation length of fluctuations ξ as compared to the polymer segmental length b (the lattice site). For correlation lengths ξ larger than the lattice sites, random positioning is no longer consistent, and more advanced theories that self-consistently include the effect of thermal composition fluctuations are needed.

The thermal composition fluctuations tend to stabilize the "disordered" phase, giving rise to a renormalized critical temperature. The relation between the mean-field value T_c^{MF} and the real T_c is expressed by the Ginzburg relation [8]:

$$T_c^{\mathrm{mf}} = T_c/(1 - G), \tag{7.88}$$

where G is the Ginzburg number. In a plot showing the inverse forward scattering $I^{-1}(0)$ versus reciprocal reduced temperature, τ^{-1}, the Ginzburg number clearly appear as the crossover temperature from linear (mean field) to nonlinear characteristics. Here, the reduced temperature is defined as $\tau = |1 - T_c/T|$. For critical composition $\phi = \phi_c$, analogous to those of Figures 7.7 and 7.8, one will find deviation from linear relationship. Polymer blends behave like classical fluids showing a three-dimensional Ising-type of scaling behavior [9,10], that is,

$$I(0) \propto \left(\frac{|T_c - T|}{T}\right)^{-\gamma} \quad \text{with} \quad \gamma = 1.24 \tag{7.89}$$

as T approaches T_c. An experimental example is provided in Figure 7.11, showing critical scattering of the polymer blend of polystyrene and polybutadiene (dPB/PS) [11,12].

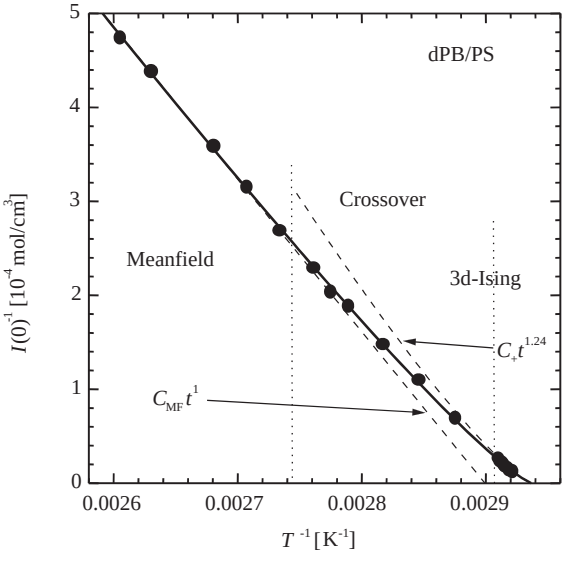

Figure 7.11 Inverse forward scattering $I^{-1}(0)$ versus inverse temperature for a mixture of dPB and PB of near critical composition. The solid line represents the best fit using the crossover function while the dotted lines shows the asymptotic mean-field and 3d-Ising laws, respectively. Adapted from Ref. [12].

Experimentally determined susceptibility, $I(0)$ versus T, like that shown in Figure 7.11, can effectively be analyzed by applying a single function describing $I(0)$ within the whole one-phase regime. Based on an ε-expansion model, one may develop a function that describes the experimental data very well [13], as seen in Figure 7.11. The parameters of the *crossover function* are the Ginzburg number, the critical temperature, and the critical exponents.

The experimental example shown in Figure 7.11 indicates clearly that the validity of the mean-field Flory–Huggins model for binary polymer blends is somewhat limited. The relevant temperature regime of most miscible polymer blends are in fact in the crossover range rather than in the mean-field, as originally anticipated. Experiments have shown that the deviation from mean-field characteristics, as expressed by the Ginzburg number, is markedly dependent on the degree of polymerization. The temperature range of non-meanfield characteristics scale as

$$|T_{mf} - T_c| \propto N^{-\alpha}, \tag{7.90}$$

with the exponent α of the order of 1 to 2 [14], but approaching a low-N value that is up to two orders of magnitude larger than that of classical liquids. The latter is the reason that most polymers in reality obey non-meanfield characteristics. Only for polymer blends with N-values larger than approximately 1000 can one find mean-field characteristics even very close to the critical point.

7.5 Block Copolymers

Polymers are, by definition, molecules composed by a large number of small chemical units, the monomers. Above, we have discussed A- and B-*homopolymers*, assuming that all A-polymers are composed of the same single A-monomer, and B-polymers by another specific B-monomer. Such chemical equality is often the situation in synthetic polymers, as for example polyethylene purely composed of $–CH_2–$ ethylene monomers. Many natural polymers, on the other hand, are composed of several different monomers; example of these include proteins, which are polymeric chains composed of different amino acids; such polymers are termed *copolymers*.

One important class of synthetic copolymers is composed of two different monomers which, in the general discussion, will be abbreviated A and B. The A and B segments may be positioned randomly within the chain, or in "blocks" of respectively A and B. Diblock copolymers composed of two linear polymer blocks linked covalently together are the most simple of this class. Diblock copolymers are closely related to blends of homopolymers; both systems are composed of two linear polymer chains, but the covalent bond between the A- and the B-blocks has of course significant implications on the physical properties.

Polymers of different chemistry are generally not miscible, as discussed above. The A- and B-molecules of an AB-diblock copolymer melt will therefore tend to cluster into domains rich in respectively A and B units. In opposition to polymer

blends, the bond between the A and B blocks prevents macroscopic phase separation. The clustering of block copolymers is therefore restricted to the nanometer length scale of the polymer blocks: they form a *micro phase-separated* state.

In diblock copolymer melts, the free energy of a micro-phase-separated state can be shown to favor ordered domain structures where the mutual organization of A- and B-domains form regular lattices. The equilibrium structure depends on the relative size of the respective polymer blocks, the overall polymer size and the temperature (or rather the product χN of the Flory–Huggins interaction parameter and the degree of polymerization).

The phenomenological theory of block copolymers is quite analogous to that of polymer blends, discussed above. The thermodynamic properties are also here determined as an interplay between configurational entropy and enthalpic contributions according to the Flory–Huggins model of the Gibbs free energy (see Section 7.3; see also Ref. [15]). It should be emphasized however that, thermodynamically, block copolymer melts are single-component system, independent of any local structural features.

Let us consider an AB-diblock copolymer with volume fraction f of A-segments and $(1-f)$ of B-segments. With the total diblock degree of polymerization (or rather number of Kuhn segments) N, each chain will have

$$\begin{array}{ll} N_{\mathrm{A}} = fN & \text{A-segments} \\ N_{\mathrm{B}} = (1-f)N & \text{B-segments} \end{array} \tag{7.91}$$

As in the development of the RPA equations for polymer blends, we will assume a uniform mixing of the A- and B-blocks, and consider the response on the spatial distribution function of A- and B-segments as a response when external fields $u_{\mathrm{A}}(\mathbf{R})$ and $u_{\mathrm{B}}(\mathbf{R})$ are applied to the system.

In the blend of homopolymers A and B, the random positioning implied that the correlation functions $\gamma_{\mathrm{AB}} = \gamma_{\mathrm{BA}} = 0$. In block copolymers, two A and B blocks are covalently bound, and the γ_{AB}-correlation term in Eq. (7.64) will accordingly not vanish. Following the arguments relating to Eqs (7.67) and (7.68) we will, when including the AB-cross terms, obtain

$$\begin{aligned} \overline{\delta\psi_{\mathrm{A}}}(\mathbf{q}) &= -\frac{1}{k_B T}\left[I^{\circ}_{\mathrm{AA}}(\mathbf{q})u^{\mathrm{eff}}_{\mathrm{A}} + I^{\circ}_{\mathrm{AB}}(\mathbf{q})u^{\mathrm{eff}}_{\mathrm{B}}\right] \\ \overline{\delta\psi_{\mathrm{B}}}(\mathbf{q}) &= -\frac{1}{k_B T}\left[I^{\circ}_{\mathrm{AB}}(\mathbf{q})u^{\mathrm{eff}}_{\mathrm{A}} + I^{\circ}_{\mathrm{BB}}(\mathbf{q})u^{\mathrm{eff}}_{\mathrm{B}}\right] \end{aligned} \tag{7.92}$$

where we have defined

$$\begin{aligned} u^{\mathrm{eff}}_{\mathrm{A}} &= u_{\mathrm{A}} - z[\varepsilon_{\mathrm{AA}}\overline{\delta\psi_{\mathrm{A}}}(\mathbf{q}) + \varepsilon_{\mathrm{AB}}\overline{\delta\psi_{\mathrm{B}}}(\mathbf{q})] + V \\ u^{\mathrm{eff}}_{\mathrm{B}} &= u_{\mathrm{B}} - z[\varepsilon_{\mathrm{AB}}\overline{\delta\psi_{\mathrm{A}}}(\mathbf{q}) + \varepsilon_{\mathrm{BB}}\overline{\delta\psi_{\mathrm{B}}}(\mathbf{q})] + V \end{aligned} \tag{7.93}$$

Combining this with the $\overline{\delta\psi_{\mathrm{A}}} + \overline{\delta\psi_{\mathrm{B}}} = 0$ restriction, we can in analogy with derivation for blends in Section 7.4.2, solve the equations for diblock copolymers and get the result:

$$\overline{\delta\psi_{\mathrm{A}}}(\mathbf{q}) = \frac{1}{k_B T}\left[\frac{I^{\circ}_{AA}(\mathbf{q}) + I^{\circ}_{BB}(\mathbf{q}) + 2I^{\circ}_{AB}(\mathbf{q})}{I^{\circ}_{AA}(\mathbf{q})I^{\circ}_{BB}(\mathbf{q}) - \left(I^{\circ}_{AB}(\mathbf{q})\right)^2} - 2\chi\right]^{-1}(u_{\mathrm{A}} - u_{\mathrm{B}}) \tag{7.94}$$

which, in analogy with Eq. (7.77), may be rewritten into the form

$$\overline{\delta\psi_A}(\mathbf{q}) = \frac{1}{k_B T}\frac{N}{F_{\text{diblock}}(\mathbf{q}) - 2\chi N}(u_A - u_B) \tag{7.95}$$

with

$$F_{\text{diblock}}(\mathbf{q}) = \frac{1}{N}\frac{I^{\circ}_{AA}(\mathbf{q}) + I^{\circ}_{BB}(\mathbf{q}) + 2I^{\circ}_{AB}(\mathbf{q})}{I^{\circ}_{AA}(\mathbf{q})I^{\circ}_{BB}(\mathbf{q}) - \left(I^{\circ}_{AB}(\mathbf{q})\right)^2} \tag{7.96}$$

which is similar to the corresponding F-function for polymer blends (Eq. (7.78)), except for the AB-cross-terms. We will assume that the diblock copolymer in the homogeneous state obeys Gaussian statistics similar to the linear homopolymers discussed above (Eq. (7.22)). The partial structure factor I°_{AA} of the individual block copolymer can then be expressed as

$$I^{\circ}_{AA}(\mathbf{q}) = \frac{1}{N}\int_0^{N_A}\int_0^{N_A} \exp\left[-\frac{b^2}{6}|n-m|\right] dn\, dm = Nh(f, N, q) \tag{7.97}$$

where $h(f, N, q)$ is a generalized Debye-function given by

$$h(f, N, q) = \frac{2}{x^2}\left[fx + e^{-fx} - 1\right] \quad \text{with} \quad x = q^2 R_g^2 \tag{7.98}$$

A corresponding calculation gives the partial structure factor I_{BB}

$$I^{\circ}_{BB}(\mathbf{q}) = Nh(1-f, N, q) \tag{7.99}$$

The partial structure factor I_{AB} for the diblock copolymer is correspondingly

$$I^{\circ}_{AB}(\mathbf{q}) = \frac{1}{N}\int_0^{N_A}\int_{N_A}^{N} \exp\left[-\frac{b^2}{6}|n-m|\right] dn\, dm$$

giving

$$I^{\circ}_{AB}(\mathbf{q}) = \frac{N}{2}[h(1, N, q) - h(f, N, q) - h(1-f, N, q)] \tag{7.100}$$

Substituting these results into Eq. (7.94) gives the RPA-structure factor for a diblock copolymer melt

$$I(\mathbf{q}) = \frac{N}{F_{\text{diblock}}(f, N, \mathbf{q}) - 2\chi N} \tag{7.101}$$

which has the same form as that of the blend given in Eq. (7.77), but with another F-function:

$$F_{\text{diblock}}(f, N, \mathbf{q}) = \frac{h(1, N, \mathbf{q})}{h(f, N, \mathbf{q})h(1-f, N, \mathbf{q}) - \frac{1}{4}[h(1, N, \mathbf{q}) - h(f, N, \mathbf{q}) - h(1-f, N, \mathbf{q})]} \tag{7.102}$$

The structure factor Eq. (7.101) with F given by Eq. (7.102) was originally derived by Leibler [15]. The structure factor approaches zero for both $q \to 0$ and $q \to \infty$, and has a distinct maximum at a q^*-value reflecting the overall size of the copolymer, and which can be calculated from the derivative: $dI(q)/dq = 0$. For

symmetric block copolymers, $f = 0.5$, this gives

$$q^* \simeq 1.945/R_g \tag{7.103}$$

The scattering function at $q = q^*$, $I(q^*)$, markedly depends on the interaction parameter χ, and diverges according to Eq. (7.101) at the critical value χ_c:

$$\chi_c \equiv \frac{F(f, N, \mathbf{q}_\circ)}{2N}, \tag{7.104}$$

which with $\chi \sim 1/T$ corresponds to a critical temperature T_c. Beyond T_c the block-copolymer system is unstable and will phase-separate on the length scale of the polymer coils: so-called micro-phase separation. The critical temperature $T_c$corresponds to the spinodal point for polymer blends.

Figure 7.12 shows examples of experimental $I(q)$ as measured at different temperature and fits using the analytical Leibler function. The experimental data are indeed fitted very well by the structure factor of the RPA theory. The solid curves shown in the figure represents best fits convoluted by the experimental resolution function. In the insert is shown the effect of instrumental smearing. In typical data analysis, both the polymer radius of gyration R_g and the Flory–Huggins interaction parameter χ are used as adjustable parameters.

Plotting the inverse of the peak-value, $I^{-1}(q^*)$, as a function of reciprocal temperature, T^{-1} (or interaction parameter χ) one should, according to the mean-field treatment, obtain a straight line in analogy with the $I^{-1}(0)$-susceptibility of blends, Eq. (7.87), which approaches zero at the critical point, here the spinodal temperature. For symmetric block copolymers, $f = 0.5$, Eqs (7.101) and (7.102) lead to the critical value, $\chi_c N$:

$$\chi_c N = 10.495, \tag{7.105}$$

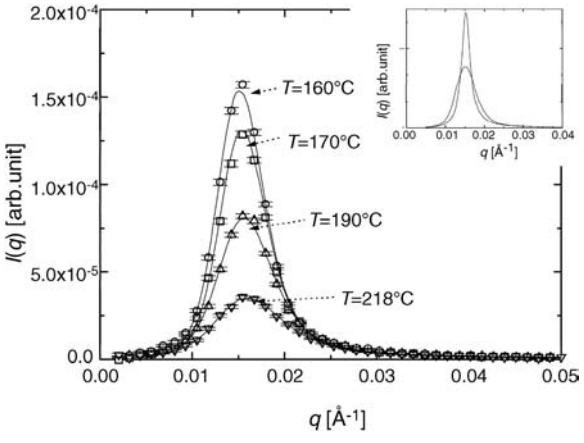

Figure 7.12 Example of experimental scattering function of a diblock copolymer, and fits using the meanfield RPA theory (solid line). The fits represent the model function including instrumental smearing. The effect of smearing is shown in the insert, giving the resulting Leibler function at 160 °C, with and without smearing.

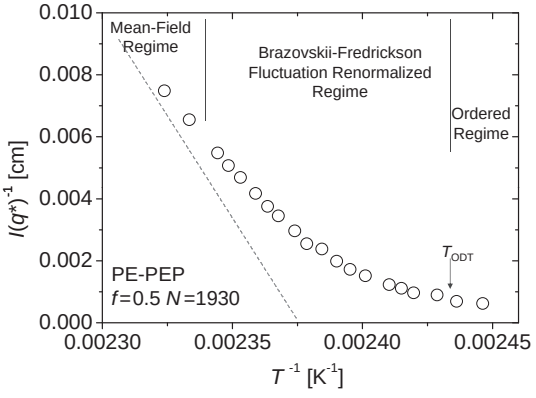

Figure 7.13 Experimental susceptibility given by the maximum value of the scattering function: $I^{-1}(q^*)$ plotted versus inverse temperature. The data illustrates the marked influence in the fluctuation renormalization near the T_{ODT}. The figure shows data of a symmetric PE-PEP diblock copolymer with $N = 1930$. Experimental data adapted from Ref. [17].

which may be compared with the corresponding critical value of symmetric, $N_A = N_B$ binary blends (Eq. (7.41)): $\chi_c N = 2$.

The mean-field theory of Leibler agrees very well with experimental observations based on X-ray and neutron scattering when obtained relatively far from the microphase separation temperature (MST). In the vicinity of the MST, however, mean-field treatment is less accurate. Both, Leibler and Fredrickson and Helfand noted that the effective Hamiltonian appropriate for diblock copolymers is in the Brazovskii-universality class [15,16]. Based on the Hartree treatment used in the Brazovskii theory, Fredrickson and Helfand found that the structure factor can still be written as the mean-field expression Eq. (7.101), but with renormalized values $\tilde{\chi}$ and $\tilde{N}$ [16]. The fluctuation renormalization makes the order parameter $I^{-1}(q^*)$ nonlinear in χ, and thereby nonlinear in T^{-1}. This is shown in the experimental example given in Figure 7.13.

7.5.1 Ordered Phases

Until now, we have discussed the disordered phase in some detail, but have not really mentioned phase behavior beyond the point where the order-parameter diverges. In fact, block copolymers do not reach the critical point, but rather undergo a weak first-order phase transition into a mesoscopic ordered structure. A significant amount of the attention paid to block copolymers in recent years has been concerned with these self-assembled microstructures. Various geometries occur, depending on the volume fraction, f, the mismatch in entropic stretching energy of the different blocks, and the degree of fluctuations as manifested through the degree of polymerization, N [18].

Most theoretical models that have been proposed are effectively based on hard core interactions by implementing the incompressibility constraint where the

average segment concentration is forced to be uniform. The remaining interactions are assumed to be local. The thermodynamic stable phases are determined by minimizing the free energy density for a given χN-value. With this approach, Leibler determined the stability of the classical ordered structures and the condition for mesophase transitions. In the symmetric $f = 0.5$ case, the transition should be of second order, going from the disordered directly to the lamellar structure. For $f \neq 0.5$, the transition is weakly first order. In the very near vicinity of the disordered phase, the minority component forms spherical micellar domains that are arranged on a bcc lattice with the matrix consisting of the majority component. Upon a further decrease in T(increase in χN), the mean-field RPA predicts a first-order transition to the hexagonal-ordered phase, where cylinders are formed by the minority component. Finally, after an even further decrease in T, a first-order transition to the lamellar structure is predicted.

Leibler's studies can be mapped onto the Brazovskii Hamiltonian, allowing calculations beyond mean-field [16]. The effect of fluctuation renormalization is not only to shift the phase boundaries to larger χN-values, but also to change the second-order critical point to a line of first-order transition between the disordered and the lamellar phase. In addition, the fluctuation renormalization causes a direct transition from the disordered phase to the hexagonal rod phase. The cubic bcc phase is substantially limited to highly asymmetric block copolymer architectures, but this depends on the overall degree of polymerization. Matsen and Bates used self-consistent field theory to show the bicontinuous $Ia\bar{3}d$-symmetric gyroid structure near the order–disorder transition regime located between the hexagonal and lamellar phases [19].

The experimental challenge related to the ordered block copolymer structures concerns the unique crystallographic identification of the phases, and also verification of the stability of an apparent observed ordered nanostructure. Since the characteristic dynamics of high-molar-mass polymer systems is often very slow, it is very difficult to conclude that an observed ordered phase is thermodynamically stable. A crystallographic description of the ordered structure has, in principle, to be solved much like the investigation of any classic crystal, but the large length scale and the amorphous building units will, of course, provide a number of special features.

Small-angle X-ray and neutron scattering has been used to solve the ordered microstructures of block copolymers. By identifying the sequence of Bragg-reflections, the ordered structure can be identified according to standard crystallographic tables. The relative intensity of the different Bragg-peaks can further be used to obtain information beyond just the ordering symmetry. Typical block copolymer samples show, however, usually only rather weak higher-order reflections; this is both a result of relative low coherence of many ordered phases, paracrystallinity, and due to the intrinsic structural characteristics. The building blocks of the block copolymer have sizes comparable to the lattice distance, causing major reductions in the intensity of the high-order reflections. Moreover, the concentration profile – and thereby the profile of the scattering contrast – has near the order–disorder transition close to sinusoidal profile. With the scattering function being the Fourier transform of the contrast profile, such a sinusoidal profile will give a significant intensity only in the first harmonics.

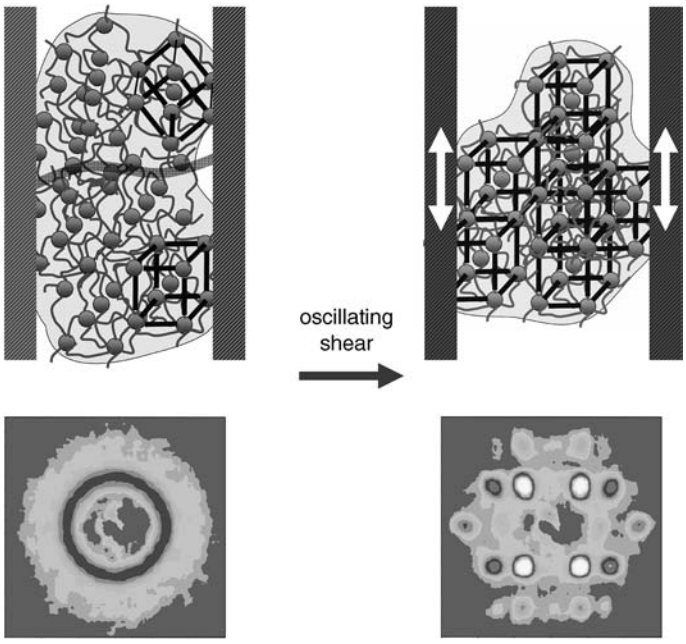

Figure 7.14 Schematic illustration of shearing a block copolymer into single domain texture, and the corresponding SANS scattering pattern.

Insight into structures can be significantly improved if the polymer sample is first transformed into a single-domain texture, and this may be achieved by applying an appropriate field. *Shear* has, in particular, been proven to be excellent for determining field-induced bulk orientation, and the shear set-up and corresponding experimental SANS pattern are shown in Figure 7.14. Specific domain-orientations may even be controlled by using appropriate shear amplitude and frequency [20]. This is shown in the experimental shear-diagram in Figure 7.15, which illustrates the characteristic texture of a polystyrene–poly(ethylene propylene)–polystyrene block copolymer network.

SANS experiments with shear-aligned samples have been used to reveal the block copolymer *phase diagram*. As each diblock copolymer is, from a thermodynamic aspect, principally a one-component system, it may be formulated as a diagram of ordered microstructures given as a function of the volume fraction of the block copolymer component, f, and the product of the degree of polymerization (N) and the interaction parameter (χ) (which is proportional to the reciprocal temperature) [18,21]. Beyond the classical phases, these experimental diagrams show lamellar, hexagonal and bcc, as well as bicontinuous $Ia\bar{3}d$, and modulated lamellar structures. An example of an experimental block-copolymer phase diagram, as obtained from SANS studies of a large variety of synthesized polystyrene–polyisoprene diblock copolymers, is shown in Figure 7.16 [18,21]. Examples of experimental scattering patterns revealing the different ordered phases are provided in Figures 7.14 and 7.15.

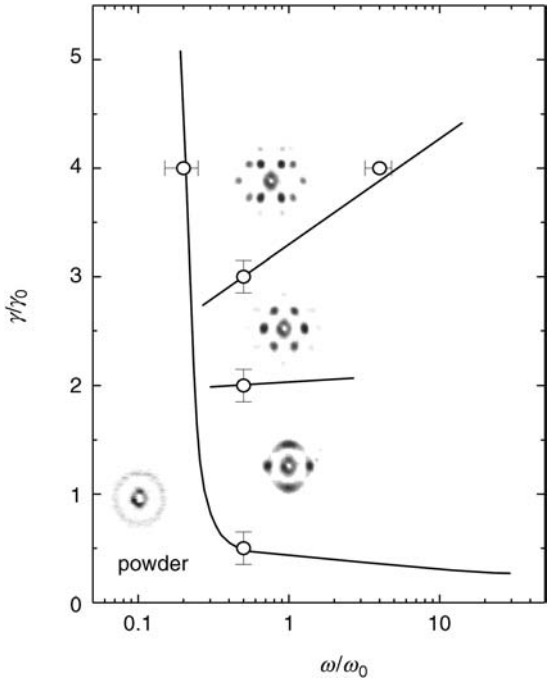

Figure 7.15 The texture of ordered diblock copolymers can be controlled in great detail applying shear with given shear-amplitude γ and shear-frequency ω. Adapted from Ref. [20].

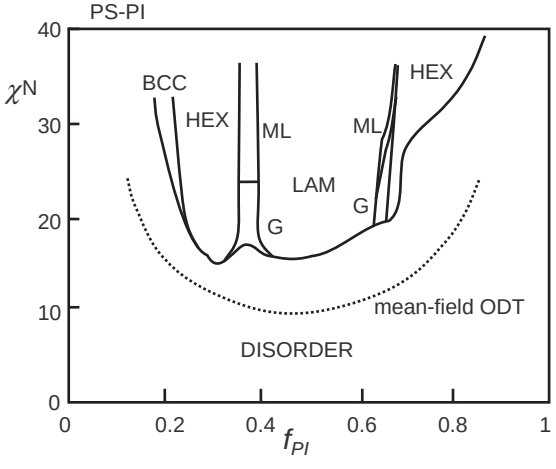

Figure 7.16 Experimental phase diagram of a diblock copolymer melt: polystyrene–polyisoprene (PS-PI) [21], showing disordered regime and five ordered microstructures: lamellar (LAM); hexagonally ordered cylinders (HEX); bodycentered cubic (BCC); modulated lamellar (ML); bicontinuous gyroid phase (G) [20].

References

1 Doi, M. (1996) *Introduction to Polymer Physics*, Clarendon Press, Oxford.
2 Flory, P. (1953) *Principles of Polymer Chemistry*, Cornell University Press, New York.
3 Higgins, J. and Beno, H. (1994) *Polymers and Neutron Scattering*, Clarendon Press, Oxford.
4 deGennes, P. (1970) Theory of x-ray scattering by liquid macromolecules with heavy atom label. *Le J. Phys-Paris*, **31**, 235–238.
5 Landau, L. and Lifshitz, E. (1980) *Statistical Physics*, Pergamon Press, New York.
6 Schwahn, D., Mortensen, K., Springer, T., Yee-Madeira, H., and Thomas, R. (1987) Investigation of the phase diagram and critical fluctuations of the system polyvenylmethylether and d-polystyrene with neutron small angle scattering. *J. Chem. Phys.*, **87**, 6078–6087.
7 Brereton, M., Fischer, E., Herkt-Maetzky, C., and Mortensen, K. (1987) Neutron scattering from a series of compatible polymer blends: Significance of the flory χ_f parameter. *J. Chem. Phys.*, **87**, 6144–6149.
8 Goldenfeldt, N. (1992) *Lectures on Phase Transitions and the Renormalization Group*, vol. **85**, Frontiers in Physics, Addison-Wesley, New York.
9 Schwahn, D., Mortensen, K., and Yee-Madeira, H. (1987) Mean-field and Ising critical behavior of a polymer blend. *Phys. Rev. Lett.*, **58**, 1544–1546.
10 Bates, F.S., Rosedale, J.H., Stepanek, P., Lodge, T.P., Wiltzius, P., Fredrickson, G.H., and Hjelm, R.P. (1990) Static and dynamic crossover in a critical polymer mixture. *Phys. Rev. Lett.*, **65**, 1893–1896.
11 Frielinghaus, H., Schwahn, D., Mortensen, K., Willner, L., and Almdal, K. (1997) Pressure and temperature effects in homopolymer blends and diblock copolymers. *J. Appl. Crystallogr.*, **30**, 696–701.
12 Schwahn, D. and Mortensen, K. (2000) Thermal Composition Fluctuations in Polymer Blends studied with Small-Angle Neutron Scattering, in *Scattering in Polymeric and Colloidal Systems*, (eds W. Brown and K. Mortensen), Gordon & Breach Science Publ., Amsterdam, The Netherlands, pp. 371–412.
13 Anisimov, M., Kiselev, S., Sengers, J., and Tang, S. (1992) Crossover approach to global critical phenomena in fluids. *Physica A: Statistical Mechanics and Its Applications*, **188**, 487–525.
14 Schwahn, D., Meier, G., Mortensen, K., and Janssen, S. (1994) On the n-scaling of the Ginzburg number and the critical amplitudes in various compatible polymer blends. *J. Phys. II (France)*, **4**, 837–848.
15 Leibler, L. (1980) *Macromolecules*, **13**, 1602–1617.
16 Fredrickson, G.H. and Helfand, E. (1987) Fluctuation effects in the theory of microphase separation in block copolymers. *J. Chem. Phys.*, **87** (1), 697–705.
17 Rosedale, J.H., Bates, F.S., Almdal, K., Mortensen, K., and Wignall, G.D. (1995) Order and disorder in symmetric diblock copolymer melts. *Macromolecules*, **28**, 1429–1443.
18 Bates, F., Schulz, M., Khandpur, A., Förster, S., Rosedale, J., Almdal, K., and Mortensen, K. (1994) Fluctuations, conformational asymmetry and block-copolymer phase-behavior. *Faraday Discuss.*, **98**, 7–18.
19 Matsen, M. and Bates, F. (1996) Unifying weak- and strong-segregation block copolymer theories. *Macromolecules*, **29**, 1091–1098.
20 Mortensen, K. (2004) Three-dimensional crystallographic determination of the body-centered-cubic morphologies of shear-aligned block copolymer systems. *J. Polym. Sci., Part B: Polym. Phys.*, **42**, 3095–3101.
21 Khandpur, A., Förster, S., Bates, F., Hamley, I., Ryan, A., Bras, W., Almdal, K., and Mortensen, K. (1995) Polyisoprene-polystyrene diblock copolymer phase diagram near the order-disorder transition. *Macromolecules*, **28**, 8796–8806.